UNIVERSIDADE DE SÃO PAULO

ESCOLA POLITÉCNICA

PAULA TIEMI GOTO

Synthesis and characterization of Co-Si and Co-ZnO thin films and nanoparticles

São Paulo

2020

PAULA TIEMI GOTO

Synthesis and characterization of Co-Si and Co-ZnO thin films and nanoparticles

Undergraduate thesis presented to the
Graduate Program at the Escola Politécnica,
Universidade de São Paulo

Concentration area:
Materials Engineering

Advisors:
Prof. Dr. Alexandre Nominé
Prof. Dr. André Tschiptschin

São Paulo

2020

Catalogação na publicação

Goto, Paula Tiemi

Synthesis and characterization of Co-Si and Co-ZnO thin films and nanoparticles / P. T. Goto – São Paulo, 2020.

47 p.

Trabalho de Formatura – Escola Politécnica da Universidade de São Paulo. Departamento de Engenharia Metalúrgica e de Materiais.

1.Thin films 2.Nanoparticles 3. Magnetron sputtering 4. Laser ablation 5.Characterization I.Universidade de São Paulo. Escola Politécnica. Departamento de Engenharia Metalúrgica e de Materiais II.t.

ACKNOWLEDGEMENTS

I would like to express my very great appreciation to my advisors Prof. Dr Alexandre Nominé (Mines Nancy/Institut Jean Lamour) and Prof. Dr André Tschiptschin (EPUSP) for the support and patience.

I am particularly grateful for the collaboration and support of Artem Larin and Dmitry Zuev from ITMO University, partner in this project with the ablation and optics. I would like to offer my special thanks to Institut Jean Lamour for allowing the use of the equipment. In particular, I thank Fahad Alnjiman, Pascal Boulet, Stéphanie Bruyère, David Horwat, Denis Mangin and Ghouti Medjahdi for the help and work with the characterization techniques. I extend my thanks to the collaborators of the materials project website which was very useful.

I would also like to thank CAPES for the Brafitec scholarship during my exchange at Mines Nancy when this project was developed.

Finally, I wish to thank also my parents and friends for encouraging me.

RESUMO

Propriedades magneto-ópticas de materiais podem permitir o controle da resposta óptica do material por meio da aplicação de um campo magnético externo. Estes materiais poderiam ser aplicados na fabricação de dispositivos para circuitos eletrônicos. Neste trabalho, o objetivo era produzir e caracterizar filmes finos e nanopartículas de Co-ZnO e Co com Si para estas aplicações. A técnica de pulverização catódica foi utilizada para a deposição dos filmes e ablação laser foi empregada para a obtenção de nanopartículas. DRX, MET, EDS e SIMS foram utilizadas no estudo de composição química e estrutura. As propriedades ópticas foram investigadas por meio de espectrometria Raman. Foi realizada com sucesso a deposição do filme fino multicamada de Co-ZnO. No entanto, as nanopartículas resultantes destes filmes finos não apresentaram as duas fases em seu interior. Uma diminuição da espessura das camadas no filme fino pode facilitar a presença de ambas fases nas nanopartículas. O filme fino de Co com Si não foi bem sucedido já que o filme não possuia uma quantidade de Si suficiente, o que explica a ausência de Si nas nanopartículas. O alvo de Si poderia estar distante demais da amostra durante a deposição do filme fino dificultando que o Si se deposite na superfície. A realização da ablação laser em vácuo poderia evitar a oxidação do Co que foi observado nas nanopartículas.

ABSTRACT

Materials with magneto-optical properties offer a way in controlling the optical response with an external magnetic field, finding application in devices for optical circuits. This study presents the synthesis method and characterization of Co-Si and Co-ZnO thin films and the nanoparticles. Thus, magnetron sputtered samples were deposited and ablation was performed on these thin films to obtain nanoparticles. XRD, TEM, EDS and SIMS were conducted to investigate the chemical composition and structure. RAMAN was used to evaluate the optical response. The results showed that Co-ZnO thin films were successfully synthesized but the resultant nanoparticles presented only one phase. Thinner layers in the thin film could promote the obtention of biphase nanoparticles. Co-Si thin films did not present enough Si which explains the absence of Si in the nanoparticles. Decreasing the distance between the target and the samples during sputtering could help in reaching the desired composition. Carrying out the ablation in vacuum should prevent the Co oxidation observed in the nanoparticles.

LIST OF FIGURES

LIST OF TABLES

TABLE OF CONTENTS

1 Introduction

Nowadays, in conventional computing, information is processed mainly with electronic circuits. Information in the form of electrons will be processed through devices such as transistors that function as logic gates.

The development of electronic technologies has been requiring an increasing data storage capacity, faster processing and improving energy efficiency. In this context, researches in optical circuits (or integrated photonic circuits) and its devices have been gaining interest in the scientific community. Instead of using electrons as information carriers, in optical circuits, the information is transmitted via photons. Therefore, photonic circuits can be 10 to 100 times faster and more energy-efficient than electronic circuits [1]. Optical circuits open doors to optical computing (Figure 1) and also for optical memories, also allowing for less energy consuming and faster writing and reading processes [2,3].

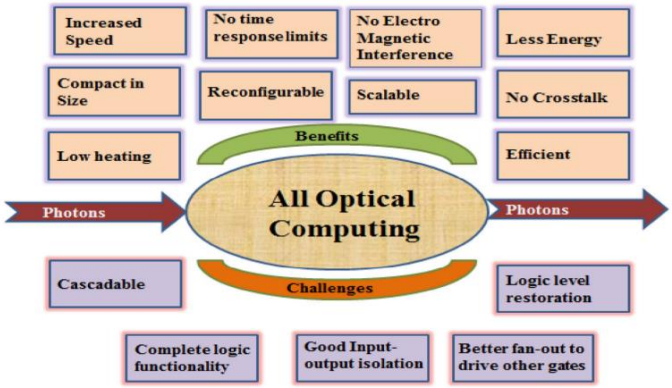

Figure 1: Benefits and challenges of all-optical computing [4].

As it was mentioned before, the photonic circuit relies on information transmission via photons. For that to occur, materials used in these circuits have to allow the control of their nonlinear optical response with an external stimulus. The nonlinear response is when there is a change in frequency, polarization, phase or path. There are various types of external stimulus that have been studied to allow the control of the optical response: via thermal [5], electrical [6], optical [7] or magnetic stimulus [8]. In this study materials with magneto-optical or magneto-photonic properties are desired. A scheme illustrating the desired properties is shown in Figure 2. The main idea is to have a non-linear material (Figure 2a) with a controllable optical response when submitted to a magnetic field (Figure

2b). Figure 2b shows a different response through a change in wavelength but in reality changes in direction, polarization, phase or path can also be envisioned.

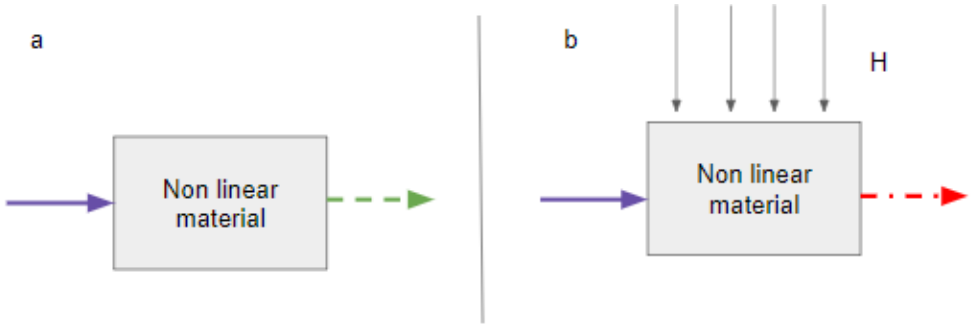

Figure 2: Scheme of the desired properties for the material. 2a: nonlinear material presenting a nonlinear response. 2b: same material under external magnetic field H with different nonlinear responses.

Considering the context of photonics and the fact that materials studied for their magneto-photonic properties are mainly presented as thin films, the objective of this work was to synthesize nanoparticles (NP) which could be used in the applications mentioned before. Having the material as NP would allow the miniaturization of devices, which is still a challenge. Besides, having the material presented as NP could enhance the optical response (explained next). In short, the idea is to obtain NP whose optical response could be modulated according to an external magnetic field.

To understand the physics envisioned in these NP for having these properties, we have first to understand the plasmon resonance. As Mie demonstrated in 1908 [9,10], the oscillation of electric and magnetic field of the light interacts with the conductive electrons of metals NP, causing them to oscillate. This phenomenon called Plasmon resonance causes high scattering and absorbance in certain wavelengths according to the NP's properties. A famous example (Figure 3) of the plasmon resonance effects is Lycurgus cup with colloidal gold and silver NP, which appears in different colours depending on the light direction. Plasmonics in high refractive index materials started gaining attention with Kuznetsov in 2012 [11], who demonstrated that these materials have smaller losses enabling stronger circular electron displacement generating a strong induced magnetic field responsible for a shift in the transmittance spectra. In Figure 4 are shown the electric magnetic field responsible for the shift in the transmittance spectra, which are similar in a metallic split-ring resonator and a high refractive index NP. Knowing the magnetic nature of the shift in the optical response, a magnetic material and the application of an external magnetic field can

increase the shift [12]. In short, the plasmon resonance allows a nonlinear response, which is enhanced in high refractive index materials and with magnetic material.

Figure 3: Lycurgus cup, plasmon resonance changing colours.

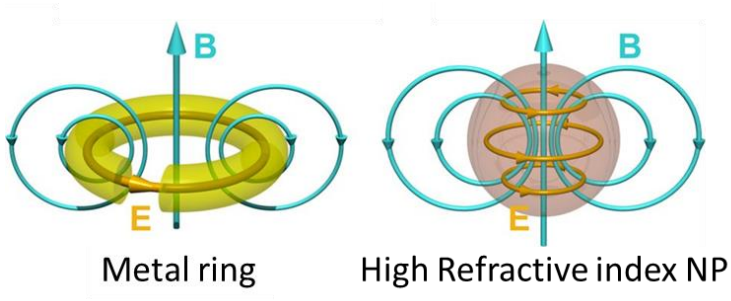

Figure 4: Representation of the electric and magnetic field in a metallic split-ring resonator and a high index material nanoparticle [11].

Taking into account the desired properties and the physics behind the planned effects, we envisioned two paths for achieving our goals. The first path consists of having a two-phase NP in which one phase is a magnetic material (ferromagnetic or ferrimagnetic), and the other is a high refractive index material. The high refractive index material will generate the induced magnetic field which will be confined and amplified by the magnetic material, enabling the amplification of the optical responses. Concerning the phase distribution in the NP, the goal is to have the magnetic material dispersed in the high refractive index material matrix forming a web. For this type of NP, we chose to work with Co as the magnetic material and with ZnO as the high refractive index material. The second path envisioned is to have a single compound NP. The material for this NP should be magnetic and be able to produce a nonlinear optical response. Non-centrosymmetric compounds are known to produce a nonlinear response. For this type of NP, we decided to search for candidates in the Co-Si system. The different possible phases in this system are shown in the literature review.

Knowing that NP presenting the desired phases may have a very specific composition range and may also be metastable, a two-step procedure was planned. First, we decided to produce thin films via magnetron sputtering. This synthesis technique is known for allowing control of chemical composition and enabling the formation of metastable phases. In a second part, these thin films would be submitted to femtosecond laser ablation allowing obtaining NP with similar compositions from the thin films and also enabling out-of-equilibrium phase due to its very fast heating and cooling rates.

At next a review of the two studied systems is presented. Then, the materials and methods used in the present work are explained. The results of the materials characterization (thin films and NP) will be shown, and at last, these results will be discussed.

2 Literature review

2.1 Co and ZnO

As it was explained in the introduction, one way envisioned to obtain NP with a nonlinear optical response is to work with a two-phase NP of Co in a ZnO matrix. The ZnO matrix, having a high refractive index, would be responsible for generating a magnetic field which will resonate and generate a nonlinear response. The role of Co, as a magnetic material is to magnify this magnetic field, amplifying the optical response.

2.1.1 ZnO: optical properties

ZnO has a high refractive index, from Kuznetsov [11] it should enable magnetic resonance shifting the response spectra, characterizing a nonlinear property. ZnO is a material that already has been studied for its optical properties. In [13], ZnO is studied for an application as nanoantennas which also require a nonlinear response, more specifically the generation of second and third harmonics (increase in wave frequency).

Since we are interested in a nonlinear optical response, one possible way of evaluating this property is via Raman Spectroscopy. Other authors such as [14] and [15] also studied the optical response of ZnO with Raman. In [14], ZnO doped with Ag and undoped NP of approximately 100nm diameter are studied for their photoluminescence. Results of their RAMAN spectroscopy result is shown in Figure 5. The peaks at 100, 380, 437 and 580 cm^{-1} correspond to fundamental phonon modes (E2L, A1(TO), E2H, and A1(LO)). The other peaks are multiphonon scattering modes.

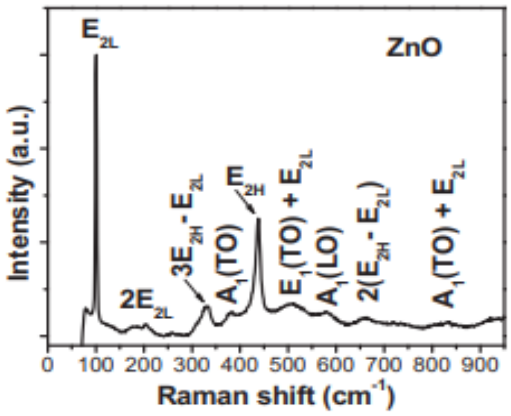

Figure 5: RAMAN spectra of ZnO NP [14].

In [15], ZnO nanocrystals doped with Co are studied with Co concentrations varying from 0 to 3 mol % that was grown at different temperatures. The spectra of their samples are shown in Figure 6. It is interesting to note that when doped with Co, we observe a shift to lower frequencies and broadening of the 440 cm^{-1} band. New bands were also found and associated with Co_3O_4 which has characteristic peaks at 483,522 and 691 cm^{-1}.

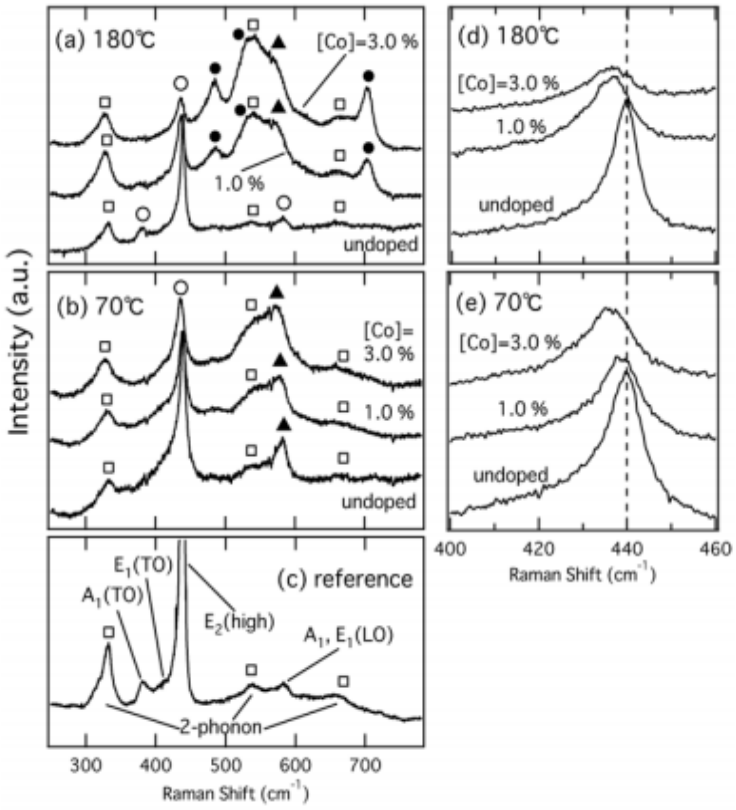

Figure 6: Raman spectra of ZnO nanocrystals doped with Co at different concentrations. (d) and (e) show peak at 440 cm^{-1} enlarged [15].

2.1.2 ZnO structure

The ZnO structure that allows such optical properties is the wurtzite structure (Figure 7). It has a hexagonal unit cell and belongs to the space group P63mc (186). It is a stable structure at room temperature and pressure.

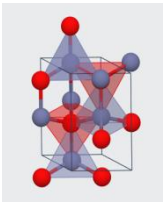

Figure 7: Unit cell of the ZnO wurtzite structure, O atoms in red and Zn in blue.

The expected ZnO x-ray diffraction pattern is shown in Figure 8. It was conducted with a diffractometer equipped using Cu Kα radiation (λ=1.5406 Å). The studied NP had sizes of 48±7 nm and crystalline size of 33±2 nm.

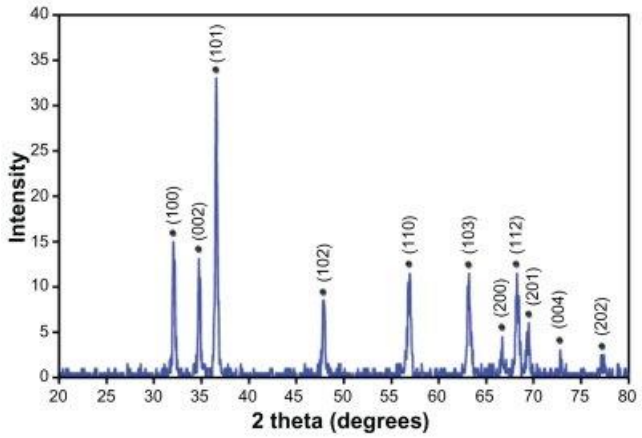

Figure 8: XRD of ZnO nanoparticles [16].

2.1.3 Co: magnetism and structure

Co is a stable ferromagnetic material with a hexagonal structure at low-temperature (ε-Co) illustrated in Figure 9. It is interesting to note that Co can easily be oxidized forming CoO which is anti-ferromagnetic. The expected XRD is shown in Figure 10. This result was obtained using Cu Kα radiation (λ=1.5406 Å). Co as a pure metal does not show characteristic peaks in Raman spectra.

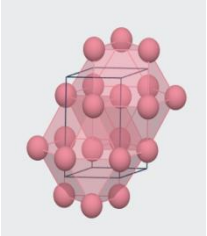

Figure 9: Cobalt hexagonal structure.

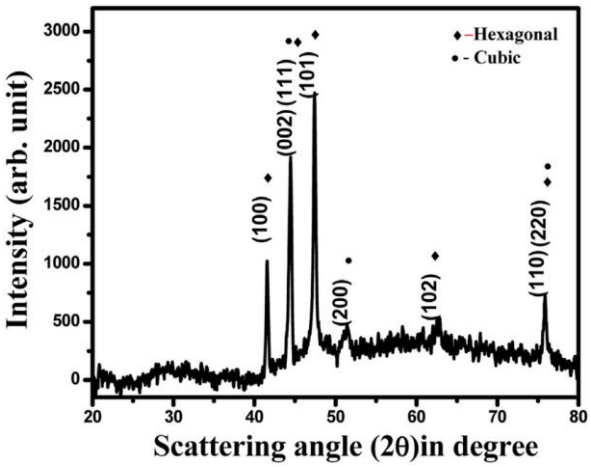

Figure 10: XRD of Co NP [17].

2.2. Co and Si system

As mentioned before, the idea with the Co-Si system is to synthesize a single-phase NP, which is non-centrosymmetric and magnetic. The magnetic material would enhance the magnetic field inside the NP, and the non-centrosymmetric structure would be responsible for generating a nonlinear response.

Thus, it is important to verify possible phases in the Co-Si system, which may present the desired optical properties.

2.2.1 Co-Si phases

The phase diagram of the Co-Si system is shown in Figure 11. As we can see, the main stable structures of Co with Si are Co_2Si, CoSi and $CoSi_2$. Among these phases, only Co_2Si is ferromagnetic. $CoSi_2$ is considered non-magnetic but present a low final magnetic moment (0.004 μ_B vs 0.016 μ_B of Co_2Si).

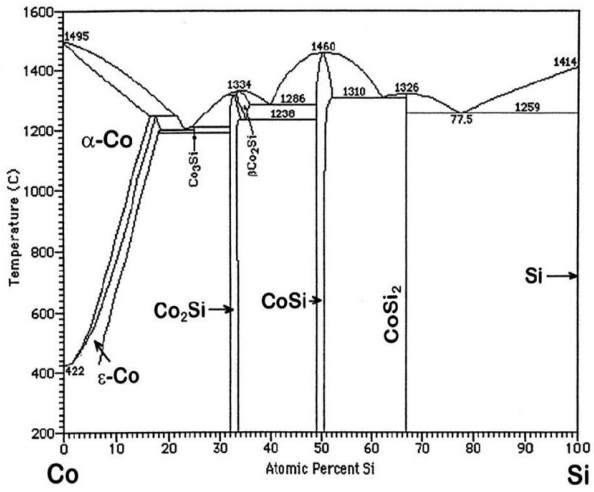

Figure 11: Co-Si phase diagram [18].

Concerning the structure, among the 3 phases, only CoSi is non-centrosymmetric. As we want the material to be both magnetic and non-centrosymmetric, none of the stable phases is desired. It is interesting to note that $CoSi_2$ does not have a characteristic Raman spectrum [19] since it has only a single weak band at 267 cm^{-1} [20]. Liu also considers that the CoSi Raman spectrum has bands at 204 and 220 $cm^{-1}$and Co_2Si presents a band at 150 cm^{-1}.

Looking also for metastable phases in the Co-Si system, we can list Co_3Si, Co_2Si_3 and CoSi (different structure). About magnetism, only Co_3Si is non-magnetic, making CoSi (metastable) and Co_2Si_3 possible candidates. For the structure requirement, only Co_2Si_3 is non-centrosymmetric, making it the desired phase.

2.2.2 Co_2Si_3

Co_2Si_3 was chosen to be the phase in the NP due to its ferromagnetism (0.399μ_B) and its non-centrosymmetric structure. This metastable compound is presented in a tetragonal structure (space group 116). The XRD for this phase was presented by Larchev [21] and is shown in Table 1.

Table 1: XRD peaks of Co_2Si_3 [21]

Number	I/I_0	d_{meas} (Å)	hkl
1	50	5.241	100
2	50	4.272	002
3	15	2.615	200
4	30	2.342	210
5	15	2.048	212
6	100	1.850	114,220
7	20	1.744	300
8	25	1.309	400,314
9	20	1.233	330

Information on the Raman spectra of the Co_2Si_3 has not been found since there are not many studies about this material. However, it is expected to obtain bands due to their non-centrosymmetric structure.

2.2.3 Co_2Si

Co_2Si is magnetic but has a centrosymmetric structure, therefore is not considered as a target structure. However, due to misunderstanding, the magnetron sputtering parameters were planned to target this structure. Some details on this compound are presented.

Co_2Si is a stable orthorhombic compound, belonging to the space group 62. The expected XRD peaks are shown in Figure 12 in blue. XRD was conducted using Co K_α (λ= 1.7889 Å). The curve in red refers to nanoclusters of Co_2Si. The peaks are located in the expected 2Θ positions but present broadening. This broadening can be attributed to the small crystallite size. Sharpness in XRD peaks is a result of destructive interference of x-rays diffracted from different planes, explaining the observed diffractogram.

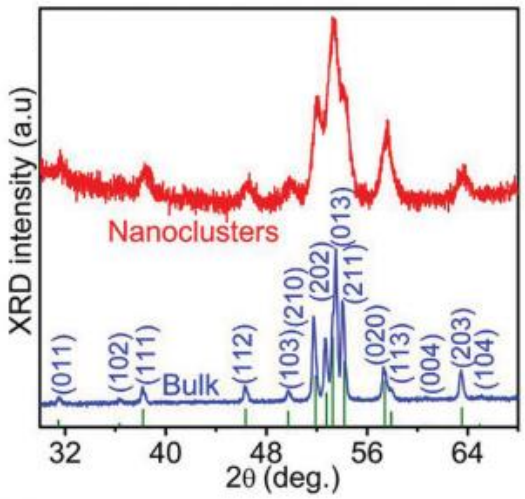

Figure 12: XRD of Co_2Si [22].

Regarding the expected RAMAN spectrum, there is a band at 150 cm^{-1}[20].

3 Experimental procedures

3.1 Overview

Two types of nanoparticles were focused :

- with a web of magnetic material (Co) in high refractive index material (ZnO)
- consisting of a single compound which is magnetic and non-centrosymmetric (Co-Si)

To obtain these NP, we conducted a 2-step process: first, thin films were deposited with the magnetron sputtering technique (Fig. 13-a), since it allows a precise composition control and the formation of metastable phases. The objective in this step was to obtain 2 types of thin films: a multilayered ZnO and Co alternated and a single layer Co_2Si. After that, the thin films were submitted to laser ablation (Fig.13-c). The laser pulse heats the sample at a high rate, producing droplets which are the NP (Fig13-d). This technique also allows the formation of a metastable phase and maintains NPs composition to those of the thin films. The overview of the synthesis and characterization of the project is shown in Figure 13.

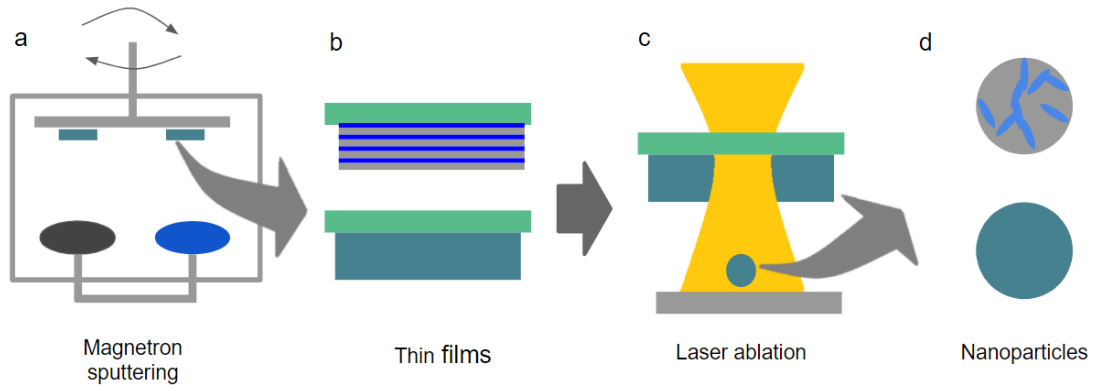

Figure 13: Overview of the project. a-magnetron sputtering for thin film deposition, b-thin films on a glass substrate: multilayered Co+ZnO and single layer Co_2Si, c-laser ablation of the thin films for obtaining NP, d-Co in ZnO matrix NP and Co_2Si NP.

3.2Thin Films sputtering

As explained, for the thin-film synthesis, the magnetron sputtering method was used. This method allows for more precise control of the chemical composition. Another beneficial aspect is that it enables the formation of metastable phases. As we have seen in the bibliography, some metastable compounds present the desired structure.

The thin films deposition was performed at Institut Jean Lamour.

3.2.1 Magnetron sputtering technique

Magnetron sputtering is a physical vapour deposition technique used for thin film deposition. The main components of magnetron sputtering equipment are the reactor chamber in vacuum, a substrate holder, a cathode, a target, a gas flow system and a power source. The gas is generally an inert gas which is ionized forming plasma. The target is negatively charged, therefore attracting the gas ions. By hitting the target, atoms are ejected. These atoms can reach the substrate holder, forming the thin film. A strong magnetic field around the target captures the gas ions, allowing more ions to collide with the target.

3.2.2 Co-ZnO thin film: sputtering

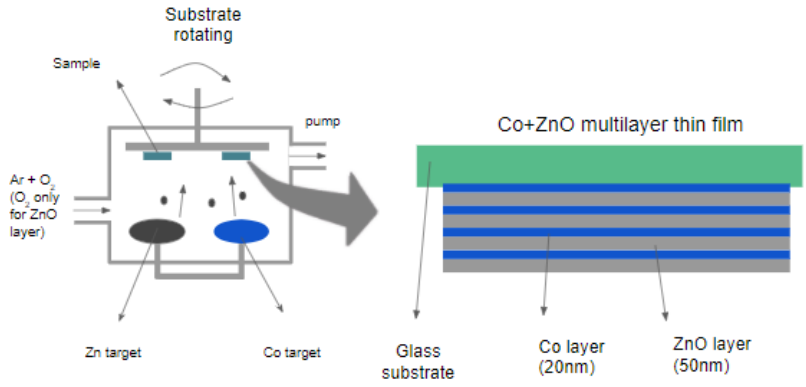

Figure 14: Co+ZnO multilayer thin film deposited with magnetron sputtering.

To have nanoparticles with a web of Co in ZnO, we synthesized at first thin films. The idea was to obtain a Co-ZnO multilayer of around 280 nm thick with 4 Co layers of 20 nm and 4 ZnO layers of 50 nm. We decided to have the first layer of Co in contact with the glass substrate because it is more heat conductive, which is important since it will be the first to have contact with the laser during the laser ablation step. We chose to leave the ZnO layer as the last one, more exposed to air since it is already oxidized. To synthesize this thin film, we used Co and Zn targets. To obtain a multilayer, each layer was deposited at a time, using different parameters.

Before sputtering, the glass substrate was cleaned with ethanol and dried with non-abrasive paper. To prepare for the sputtering, the targets were fixed at 5 cm distance from

the substrate holder. The two glass substrates were set at the tangential direction of the substrate holder disk at 7.5 cm of the rotation axis. Two substrates were fixed, so one sample would be characterized, and the other would be ablated. During sputtering, this substrate holder was kept in rotation to promote homogeneous composition. The sputtering chamber was closed and pumped to obtain vacuum overnight. Just before the beginning of the deposition, 1 minute of etching (bombardment with protection between the target and the substrate) is conducted to increase adhesion by removing a few substrate layers.

The deposition was performed at room temperature. For the Co layer, Co was sputtered with an Ar flow rate of 90 cm^3/min using a Co target. The power source was set in DC mode with a current of 170 mA, corresponding to 575 V. The pressure was $8.74.10^{-3}$ mbar. Each Co layer was sputtered for 2 min 30 s.

For the ZnO layer, reactive sputtering was used. A Zn target was employed, and it reacted with O_2. The Ar flow rate was 50 cm^3/min, and the O_2 flow rate was 10 cm^3/min. The power source was in DC mode with a current of 70 mA corresponding to 311 V. The pressure was $4.12.10^{-3}$ mbar. The time of sputtering for each ZnO layer was of 18 min. In Table 2, the parameters used are summarized. All the parameters used were determined considering previous depositions made in the laboratory.

Table 2: Magnetron sputtering parameters for Co-ZnO thin film

Parameters	Co layer	ZnO layer
Type	non-reactive deposition	reactive deposition
Target	cobalt	zinc
Ar flow (cm^3/min)	90	50
O_2 flow (cm^3/min)	x	10
Power source	DC, 170mA, 575V	DC, 70mA, 311V
Pressure (mbar)	$8.74.10^{-3}$	$4.12.10^{-3}$
Deposition time	2 min 30 s	18 min

3.2.3 Co_2Si thin film: sputtering

Considering that we planned to obtain single-phase Co_2Si NP, a single layer of Co_2Si was envisioned. The objective was to deposit a 300nm layer on a glass substrate. As it is a single layer thin film, the deposition was conducted in one step. Figure 15 presents the global procedure of Co_2Si thin film deposition as well as the desired thin film structure.

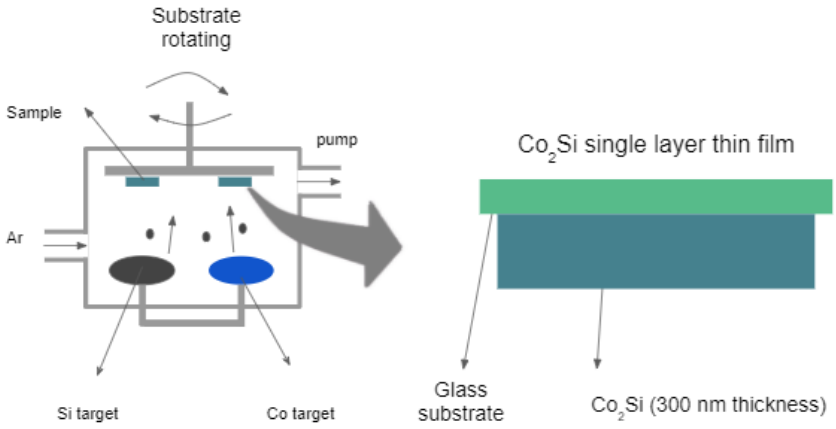

Figure 15: Co_2Si thin film deposited with magnetron sputtering.

The preparation of the substrate and the magnetron sputtering equipment followed the same procedures as for the Co-ZnO thin film deposition.

The sputtering of Co-Si thin film was also performed at room temperature. For the deposition of Co-Si thin film, the sputtering of Co and Si occurred at the same time during 20 min, using Co and Si targets. The pressure was $8.36.10^{-3}$ mbar. The Ar flow rate was set to 90 cm^3/min. For Co, the target was placed at a distance of 5 cm of the substrate. The power source was in DC mode and was regulated for 170 mA corresponding to 512V.

For Si, the target was at 10 cm from the substrate. The power source was set in the DC pulsed mode, at 369 V, 0.54 A, 290 kHz and a time off of 1.1 µs. Pulsed DC was chosen for the Si target since it presents electrical instability. The summary of the parameters is in Table 3.

Table 3: Magnetron sputtering parameters for Co-Si thin films.

Parameters	Co	Si
type	non-reactive deposition	
Target	Co	Si
Ar flow (cm^3/min)	90	
Power source	DC, 170 mA, 575 V	Pulsed DC, 0.54 A, 396 V, 290 kHz, t_{off}=1.1 µs
Pressure (mbar)	$8.36.10^{-3}$	
Deposition time	20 min	
distance target/substrate	5 cm	10 cm

Considering that the aimed composition may not be achieved, it would be incorrect to call this sample as Co_2Si thin film, and it will be simply referred to as Co-Si thin film.

3.3 Thin film characterization

For thin films characterization, X-ray diffraction (XRD) and grazing incidence X-ray diffraction (GIXRD) were conducted to have information about the structure. Diffractions were done with 2Θ from 15 to 120°. For XRD, the X-ray tube was Cu Kα (λ_{Cu}= 0.154060 nm), and for GIXRD, the X-ray tube was Co Kα (λ_{Co}= 0.17889 nm). GIXRD heating until 400°C was also performed in the Co-Si thin film to detect crystallization of eventual amorphous phases present in the thin film.

Secondary ion mass spectroscopy (SIMS) was conducted to verify the chemical composition of the thin films. This technique would allow obtaining a chemical composition distribution in thickness, which is more interesting in the case of the multilayer. In the case of the Co-Si thin film, this technique was faster to verify the presence of Si.

Raman spectroscopy was also carried out in thin films for phase identification and to verify its eventual nonlinear optical properties. For this characterization, the laser used had a wavelength of 632.8 nm coupled with a Horiba Jobin-Yvon LabRam HR800 monochromator supported with 1000 lines per mm diffraction grating, a water-cooled CCD detector (iDus DU420A-OE) in the optical range 400 – 1000 nm.

XRD, GIXRD, GIXRD with heating and SIMS were performed at Institut Jean Lamour. Raman spectroscopy was carried out at ITMO University, our partner in this project.

3.4 Nanoparticles synthesis: ablation

For the NP synthesis, the femtosecond laser ablation technique also called Laser-induced Forward Transfer (LIFT) was used. This technique is known for being used in inkjet printing and electronics [23]. An example in electronics is the deposition of light-emitting polymers in a substrate for OLED fabrication. The fabrication of NP with this method has also been investigated [24], [25].

This technique was adopted because it would allow the synthesis of NP from the thin films and enables the formation of metastable structures which can be desired for its properties. The equipment was available at ITMO University. Therefore, this step was carried out there.

In this technique, a laser pulse is focused on a donor sample promoting high energy in an area of about 5 µm. This energy is enough to cause melting or vaporization of the sample. As a result, NP are collected in a receiver substrate.

The sample is placed under the laser source, with the glass facing the laser source. Under the sample, a TEM grid is placed to collect the NP since characterization in TEM was planned. The laser ablation was conducted in the air at room temperature using femtosecond laser source (TeMa 150, Avesta Project) with an average power of 86.6 mW, repetition rate (frequency of the pulses) of 160256 Hz and an intensity of 2.83 W/cm^2. The pulse wavelength was 1050±5 nm, characterizing it as a near-infrared beam. The objective lens was set to a ten times magnification and at a numerical aperture of 0.26.

3.5 Nanoparticles: Characterization

For the NP characterization, bright field, scanning transmission electron microscopy (STEM-BF), high angle annular dark field (STEM-HADF) and transmission electron microscopy (TEM) were conducted, to get information on particle shape, phases, crystalline/amorphous phases and distribution, in a JEOL ARM 200-Cold FEG equipment available at Institut Jean Lamour.

Selected area electron diffraction (SAED) was used to identify structures of the NP. Energy dispersive spectroscopy (EDS) gave information on chemical compositions.

For optics characterization, RAMAN spectroscopy was performed using the same equipment and parameters used for the thin film characterization. Scattering spectra by dark field method was also obtained. This step was performed at ITMO University.

4 Results

4.1 Co-ZnO thin film

The XRD of the approximately 300 nm thick thin film presented a lot of noise and barely detectable peaks, turning the analysis challenging.

The GIXRD result is presented in Figure 16. The diffraction peaks were compared with the expected peaks of the hexagonal Co and the ZnO wurtzite, taken under Cu Kα radiation. d-spacings were converted to 2Θ angles using Bragg's Law (λ=2dsinΘ). The broad peak centred around 27° was attributed to the SiO_2 in the glass substrate. The ZnO (002) peak was very intense, comparing to the usual intensity of the ZnO (002) peak [16] compared to the other peaks. It can be interpreted as an epitaxial growth in (200) direction.

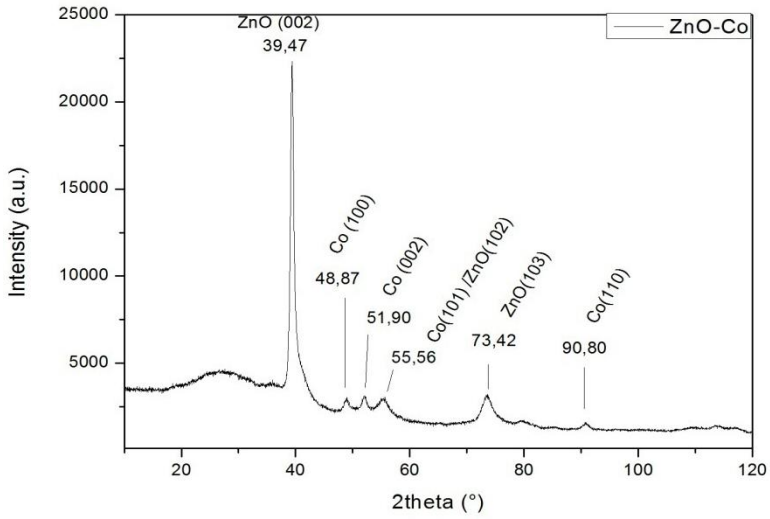

Figure 16: GIXRD of Co-ZnO thin film.

To verify the chemical composition and also to characterize the multilayer structure, SIMS was carried out. The SIMS results are shown in Figure 17, showing the intensity for each element as a function of the time. In fact, in the SIMS method, the sample is bombarded, causing the atoms in the surface to be projected. In Figure 17, time is related to depth in the sample, and the corresponding intensity depends on the content of the element in the sample.

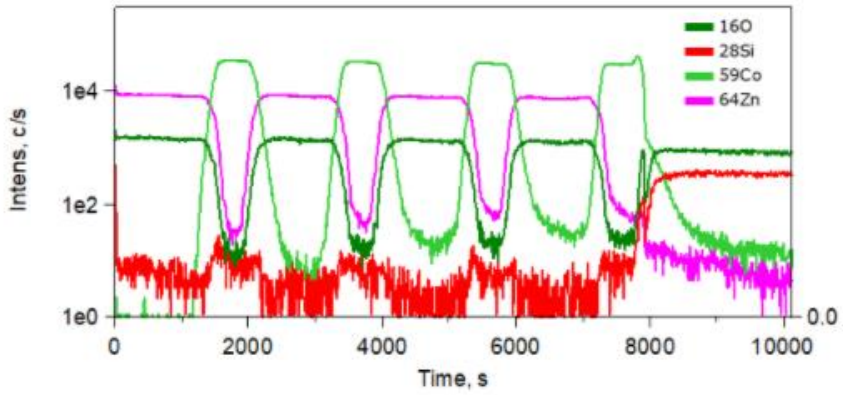

Figure 17: Co-ZnO thin-film SIMS.

It is possible to identify the four layers rich in Zn (pink) and O (dark green) and the layer with high Co content (light green). After 8000 s, Si and O were detected, which is attributed to the glass substrate. Considering the absence of Zn and Co in the substrate, we can presume that the Co content is low in the Zn rich layer and vice versa. Although the peaks and valleys are steep, we cannot assume that no diffusion occurred between layers, since layers surfaces are not perfectly plane and SIMS beam affects an area of the sample (resolution). It would be interesting to calculate the thickness of the layers. However, knowing that the sputter rates may vary with the material and orientation, it is difficult to find a reliable thickness.

Concerning the optical response, peaks from the ZnO were detected. The vibration modes at 95 cm^{-1} and 434 cm^{-1} were identified as E2L and E2H fundamental vibration modes [14]. Bands at 326 cm^{-1} and 546 cm^{-1} correspond to multiphonon vibration. As for Co, since it is presented as a pure metal, it does not show any Raman bands.

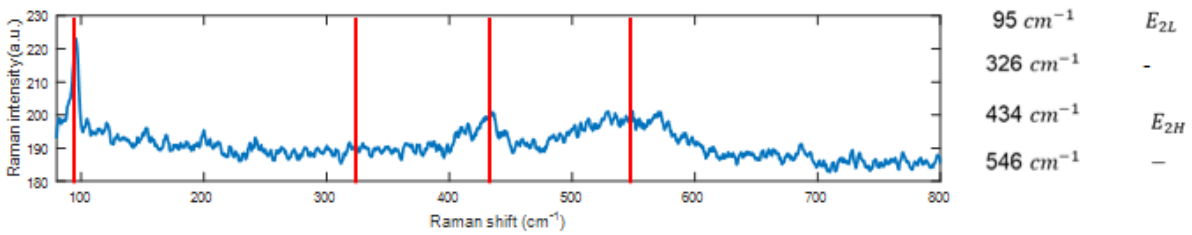

Figure 18: Raman spectrum of the Co-ZnO thin film [26].

4.2 Co-Si thin film

As well as for the Co-ZnO thin film, XRD was not exploitable. The GIXRD result is presented in Figure 19. The obtained d-spacings were compared with d-spacings found in the literature [21]; no correspondence with the Co_2Si structure was found. The peaks were attributed to the Co hexagonal structure. Since no relevant difference in the d-spacings was found compared to those in literature, we can assume that there is any or at least low distortion in the cell, which does not prove the presence of Si in the sample.

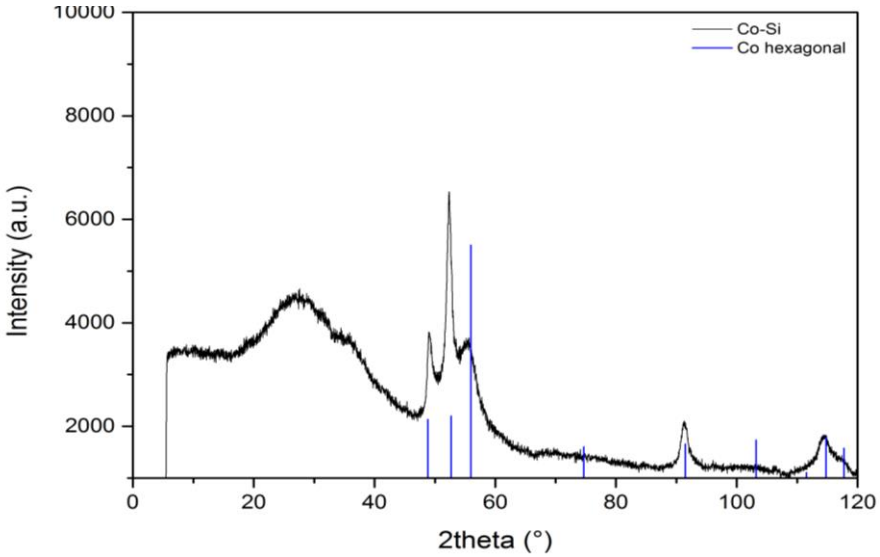

Figure 19: Co-Si thin-film GIXRD.

A hypothesis was that Si was present in amorphous form and could not be identified in the GIXRD. A first way to verify this hypothesis was to perform a GIXRD with heating, to promote crystallization. The result is shown in Figure 20. Heating GIXRD until 450°C did not show structural changes. The Co did not change to α-Co since it requires a higher temperature (Figure 11). No new diffraction peaks were identified that could be associated with Si crystallization.

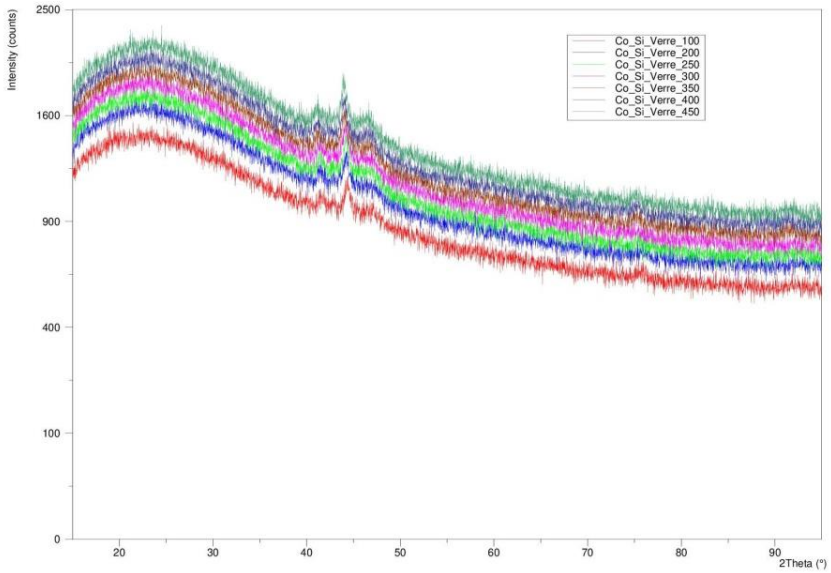

Figure 20: Co-Si thin-film heating from 100°C to 450°C GIXRD.

SIMS was then conducted to verify the presence of Si. The result is presented in Figure 21, showing the intensity in counts/s as a function of time for O, Si, Co and Cs, which was used for bombardment. It is important to note that this characterization was not performed in all of the thin film depth. The average intensity for Co was 33 ± 1.10^3 counts/s and for Si was 56±4.10 counts/s. SIMS technique can be used for element quantification, which will be discussed in section 5. It is also interesting to observe that the oxygen content is higher at the early times, showing possible oxidation.

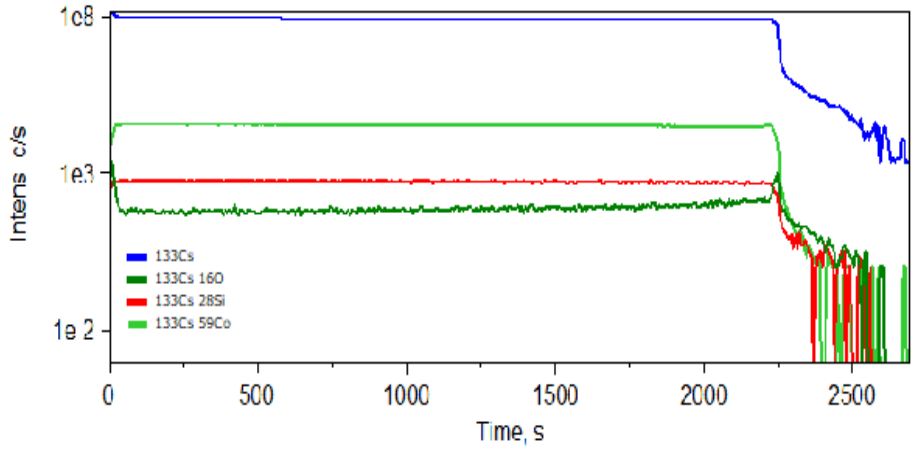

Figure 21: Co-Si thin-film SIMS.

For the optical properties, Raman spectroscopy was performed on the Co-Si thin film. However, no characteristic bands were observed. Raman was also conducted in a spot closer

to the ablation line, affected by the laser beam. The results are displayed in Figure 22. Bands were found at 193, 480, 521, 618 and 688 cm^{-1}.

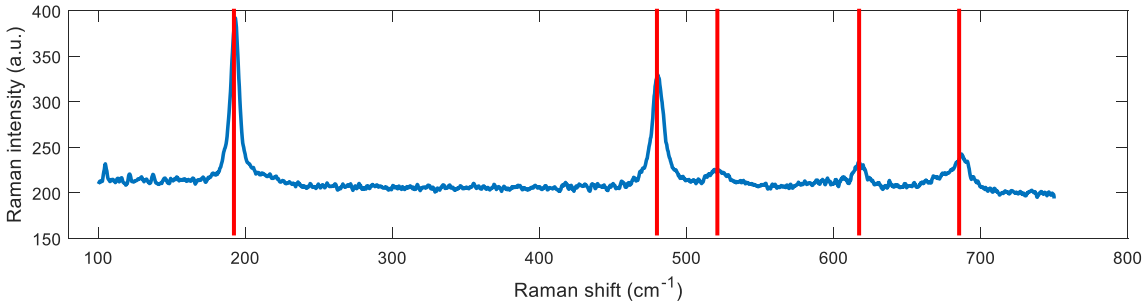

Figure 22: Raman spectra of the Co-Si thin film at the ablation line [26].

These bands were identified as vibration modes of the Co_3O_4 shown in Figure 23.

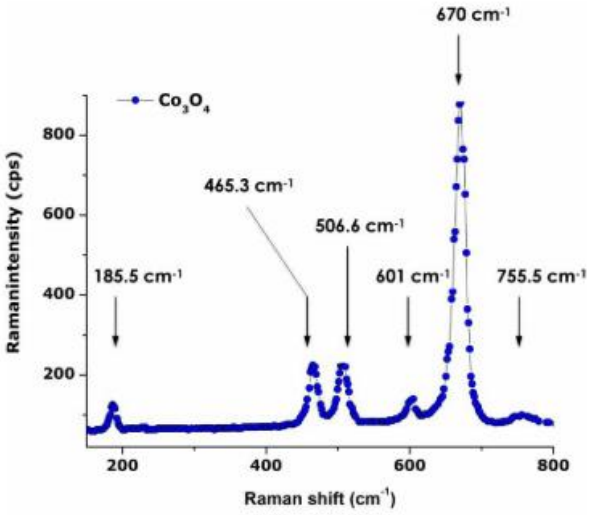

Figure 23: Raman spectra of annealed Co_3O_4 nanoparticles [27].

4.3 Co-ZnO nanoparticles

Fabrication of NPs was normally carried out on a TEM grid, but there was a problem with ablation on the glass that could be due to low adhesion.

To verify the structure, amorphous/crystalline phases and NP size and shape, TEM was performed. The grids had almost no carbon left, as shown in Figure 24, probably due to the laser ablation. Considering that, only particles that were in the marked area were analyzed.

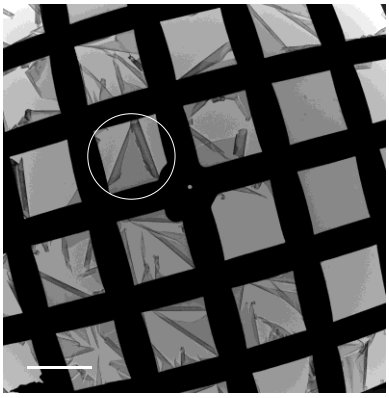

Figure 24: TEM grid with carbon film damaged.

Nanoparticles had a size of 70±20 nm.

Amorphous and crystallized phases were found. Some crystallization occurred inside the microscope, during the TEM session. For the crystallized phases, many particles showed only one family plane with an interplanar distance of d=0.25 nm. This distance could be associated with the 200 planes of the ZnO hexagonal phase found in a thin film. The TEM and the Fourier transform are shown in Figure 25.

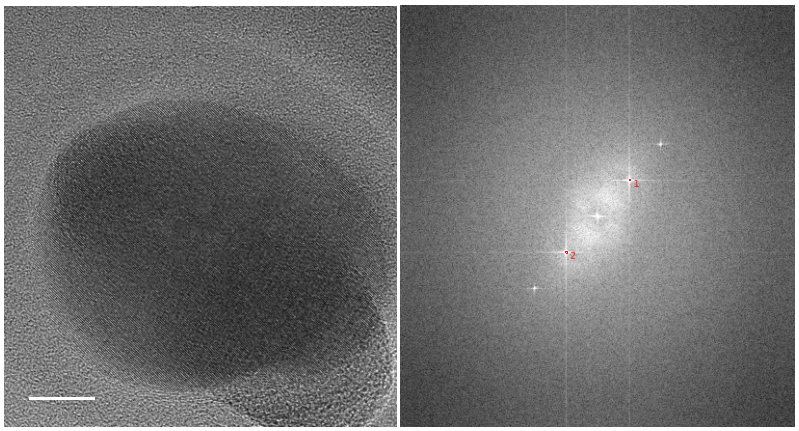

Figure 25: TEM of a Co-ZnO nanoparticle (left) with the SAED (right).

Some other particles also showed the different structure with more family planes and a different interplanar distance, that did not correspond to the d-spacing identified in the XRD of the thin film, Figure 26. The structure was not identified. The interplanar distances are presented in Table 4.

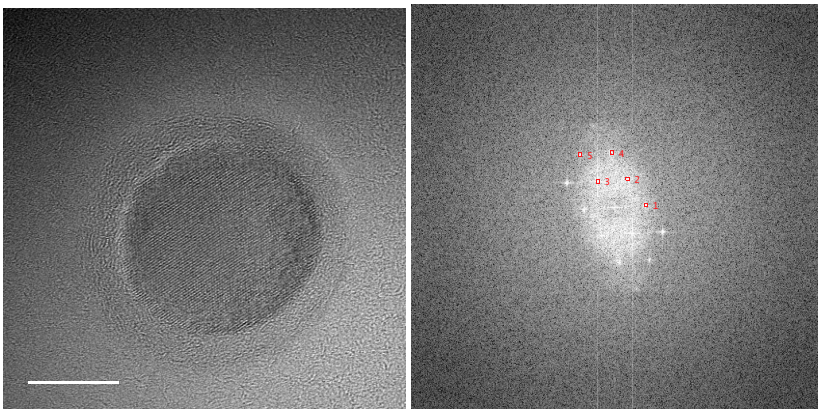

Figure 26: TEM of Co-ZnO nanoparticle (left) with the SAED (right).

Table 4: d spacings of the planes of Co-ZnO nanoparticle shown in Figure 26

Spot #	d-spacing (nm)
1	0.2836
2	0.2824
3	0.2813
4	0.1619
5	0.1399

The nanoparticles showed different chemical compositions. We observed that the bigger particles did not have Zn. A core-shell structure was found with Co at the core and oxidized Co around (Figure 27). In general, compositions were of about 50% O and from 0 to 26% Zn.

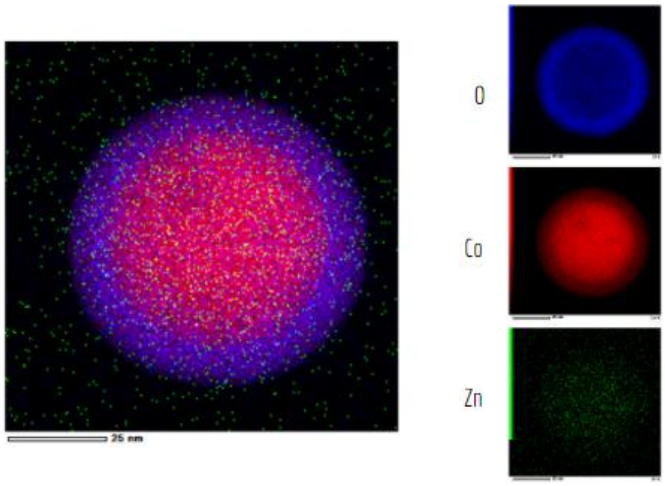

Figure 27: EDS of Core-shell structure of a Co-CoO nanoparticle.

4.4 Co-Si nanoparticles

For the chemical composition, very few Si was found (less than 0.6%). The nanoparticles containing no Si, some core-shell structures were also found of Co and Co-O in the shell.

With the TEM, we could verify that the nanoparticles showed amorphous and crystallized phases. Crystallized phases showed a Co hexagonal structure, the same found in the thin films. The TEM with the Fourier transform and the d-spacings are presented in Figure 28. The spots 3 and 4 were not associated with any plane.

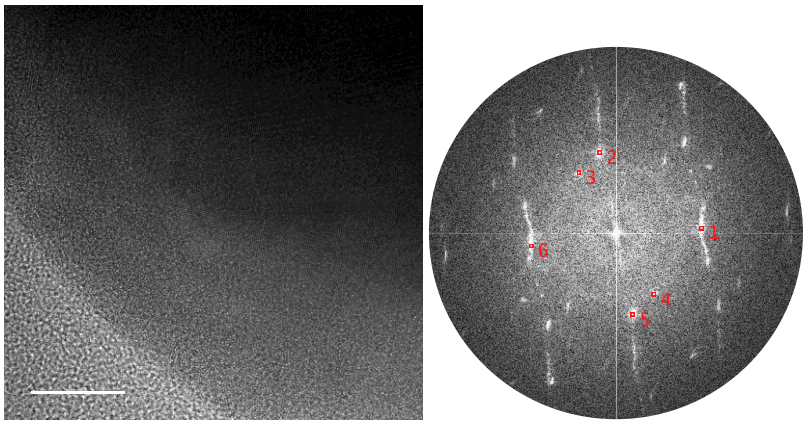

Figure 28: TEM of Co nanoparticle (left) with SAED (right).

Table 5: d spacings of the planes of Co-Si nanoparticle shown in Figure 28

Spot #	d-spacing (nm)	Associated plane
1	0.2028	Co (002)
2	0.2105	Co (100)
3	0.2431	-
4	0.2412	-
5	0.2088	Co (100)
6	0.2023	Co (002)

RAMAN spectra showed different signals corresponding to the core and shell regions of the particle. In Figure 29, the signal represented in blue was a response of the part of an NP shown in the figure with blue borders, therefore corresponding to the core. The same is valid for the red curve, which corresponds to the shell. This behaviour can be associated with the core-shell structure found previously.

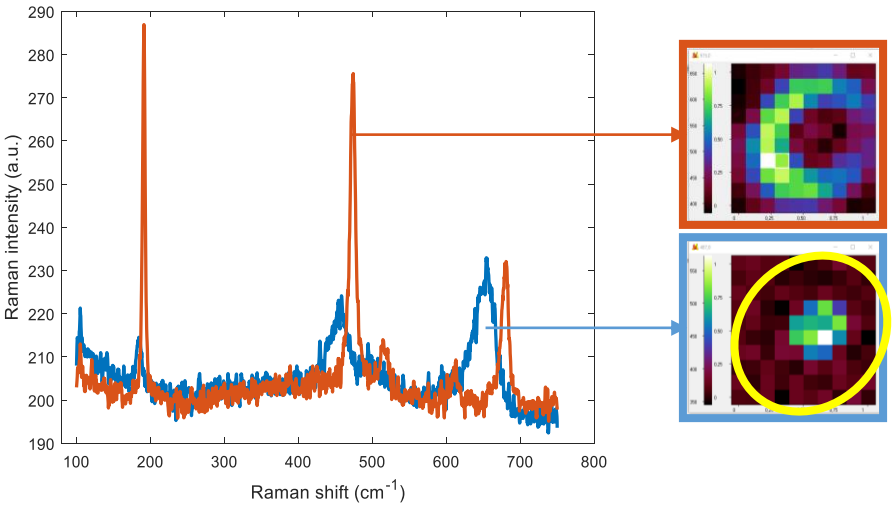

Figure 29: Raman spectra and mapping of Co-Si nanoparticle [26].

The bands found in Raman could be associated with different oxidation states of cobalt. The shell is Co_3O_4 and the core is CoO. The spectrum used as a reference to identification is shown in Figure 30.

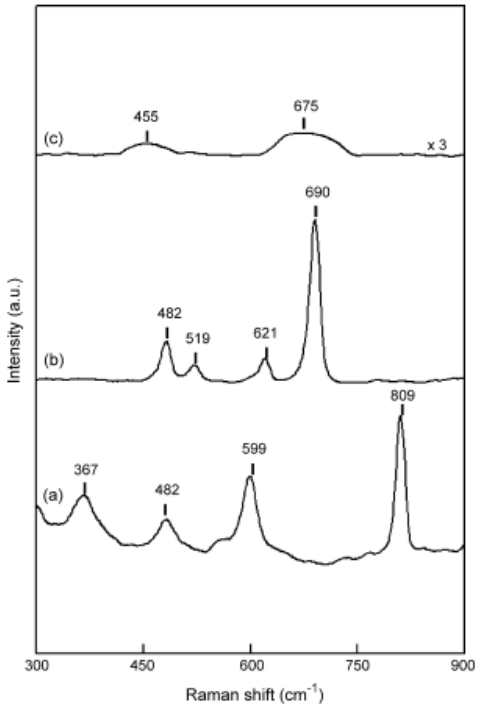

Figure 30: Raman spectra of (a) CoO(OH), (b) Co_3O_4 and (c) CoO [28].

Other results of RAMAN spectroscopy with the scattering spectra are presented in Figure 31 for other NP. The Raman spectrum shows similar bands for NP2 and NP3 with bands at 190, 480, 520 and 690 cm^{-1}. These bands are equivalent to those found in the thin film, associated with Co_3O_4. NP3 does not show strong bands. NP2 and NP3 show a similar

scattering elbow between 700 and 800 nm. It is also interesting to note a shift in the wavelength.

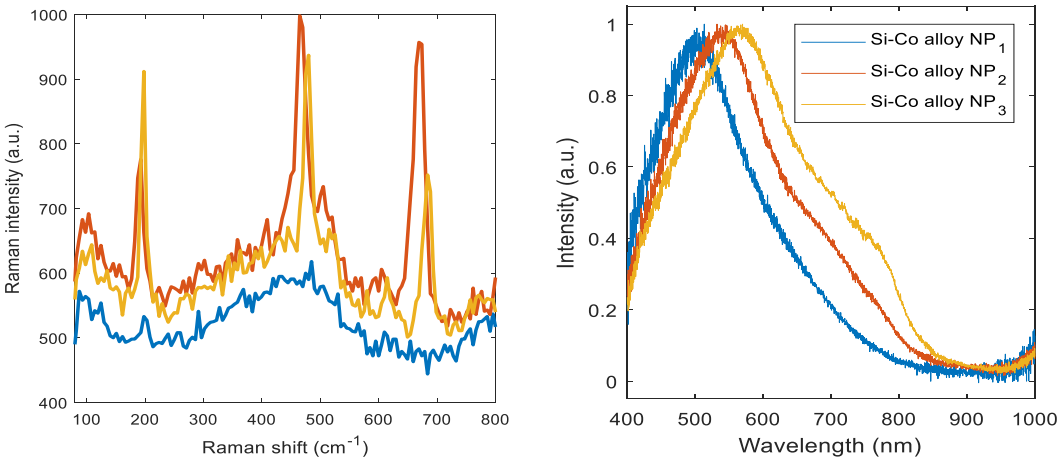

Figure 31: Raman spectra of Co-Si nanoparticles and their corresponding DF scattering spectra [26].

5 Discussion

The characterizations were made to verify if the desired material and structure were achieved in each step of the process (thin film deposition and NP ablation). A discussion of the characterization results for each system will now be made.

5.1 Co-ZnO thin film

The objective was to obtain a multilayer of four Co layers intercalated with four ZnO layers. Co should have a hexagonal structure and ZnO should present a wurtzite structure. The expected Raman would present only ZnO bands.

The SIMS result confirmed that the multilayer structure was successfully achieved. Layers were distinct with layers rich in Co and layers rich in Zn and O. The variation in the Si signal between the layers can be attributed to matrix effects. Si has not the same ionization probability when it is present in a Co or a ZnO layer. Concerning the structure, XRD showed diffraction peaks from both desired structures. A particularity of our sample is that it presented epitaxial growth in (200) direction. It is not known if this orientation could influence NP properties. Concerning the Raman spectroscopy, the sample showed the predicted behaviour.

With all the results, the deposition of the Co-ZnO thin film produced the planned structure and composition.

5.2 Co-Si thin film

The actual objective was to obtain a single layer of Co_2Si_3 which non-centrosymmetric and ferromagnetic. The structure would be tetragonal, and although no Raman spectrum of this material was found, bands were expected due to its non-centrosymmetric structure.

However, due to error, parameters on the magnetron sputtering were fixed, focusing objective of obtaining a single layer of Co_2Si. The structure would be orthorhombic,

centrosymmetric. The material should be ferromagnetic and would present a Raman band at 150 cm^{-1}.

The GIXRD detected peaks corresponding to the hexagonal Co with no sign of lattice deformation. Heating GIXRD did not show any changes in the structure until 450°C, contradicting our hypothesis of the presence of Si in an amorphous state. SIMS result shows that concentration was homogeneous along the thin film depth submitted to bombardment. Si was detected in SIMS. The possibility of equipment contamination was discarded since, usually, contaminations appear with constant intensity. In this technique, the intensity is not directly proportional to the concentration due mainly to matrix effect, which promotes ionization of some elements more than others. Models exist, enabling quantification of an element employing a relative sensitivity (RSF) coefficient dependent on the studied element and the matrix. Unfortunately, this coefficient was not found, impeding an estimation of the concentration. However, considering the other results, we can infer that the concentration of Si is around 1.7%at, far from 33%at which was the goal. The Raman spectra also confirm these results since no signal was detected, probably because the thin film was mainly Co. The Raman at the ablation line shows the oxidation of Co due to the energy furnished and air atmosphere forming Co_3O_4, with no evidence of Si.

In this step, Si sputtering was not successful. A cause may be that the target was too far from the substrate, not allowing the Si to reach the surface. A solution could be fixing the target at a smaller distance to the substrate. Besides, authors in literature have reported difficulties in performing Si sputtering at room temperature. Si presents electrical instability which is why deposition is usually carried out in pulsed DC or radiofrequency mode. Pulsed DC at low temperatures is an actual challenge. A natural solution to our problem would be to perform sputtering at 400-450°C, such as recommended by Reinig [29]. However, an increase in temperature could promote the equilibrium in the thin film, hindering the growth of metastable phases. An alternative would be to change the current to a radiofrequency mode. In [30], magnetron sputtering of Si at room temperature in RF mode at 525 W, with a frequency of 13.56 MHz and distance substrate-target of 6 cm produced successfully Si amorphous film.

5.3 Co-ZnO NP

The objective for the Co-ZnO NP was obtaining a web of Co inside a ZnO matrix. The desired structure is the same as those of the thin film: wurtzite structure of ZnO and hexagonal structure of Co. The Raman was expected to present enhanced intensity of the bands due to the Co web.

With the microscopy images, NP did not show the Co web inside a ZnO matrix. In general, NPs obtained presented crystallized and amorphous phases and were composed by either CoO with Co_3O_4 or ZnO. It is suspected that NP had more amorphous phase than seen in microscopy, considering that the beam was promoting crystallization during observation. Core-shell structure was found in particles composed mainly of oxidized Co.

Knowing that the thin film deposition occurred as planned, changes in the thin film may help in achieving the web structure of Co inside ZnO. Changes in Co thin film layer may help in the incorporation of Co in the NPs. Reducing the Co layer thickness might favour the presence of both phases in the NP. Having agglomerations of Co instead of a layer could also promote the incorporation of Co in the NP. Another parameter to be tested would be the environment of the laser ablation. Laser ablation was performed in an air environment, explaining the Co oxidation. Ablation carried out in vacuum, would prevent oxidation and more specifically, the formation of CoO which is anti-ferromagnetic, not contributing to the enhancement of optical properties. Another problem was the damage of the carbon sheet of the TEM grid making TEM microscopy difficult. A solution could be envisioned to avoid this problem.

After an eventual success in the enhancement of the non-optical properties, magneto-optical should be investigated employing Raman spectroscopy and DF scattering spectroscopy with an external magnetic field.

5.4 Co-Si NP

The objective was to obtain a non-centrosymmetric and ferromagnetic Co_2Si_3 metastable structure. The Raman spectrum should have bands enhanced in intensity compared to a Co_2Si_3 thin film, due to the surface resonance plasmon occurring in NP.

Knowing that sputtering was planned looking forward a Co_2Si structure, we could also expect obtaining Co_2Si NP although it does not have the desired optical e magnetic properties.

The NP obtained were mainly oxidized Co forming a core-shell structure of Co_3O_4 as the shell and CoO as the core. We can not affirm that all NP presented crystalline phases before the microscopy as for the Co-ZnO NP, some crystallization was observed during the investigation. The optical results went along with the other results where signals were different in the core and the shell. These results were all expected, considering that thin-film deposition failed.

Apart from changing sputtering conditions as it was discussed in 5.2, changes in laser ablation could also be envisioned. As for Co-ZnO NP, Co oxidation was observed. Laser ablation performed in vacuum should avoid oxidation.

6 Conclusion

Components for optical circuits have to present a form of control of light through an external stimulus. Magneto-optical properties of materials could allow control of the optical response with the absence or presence of an external magnetic field. This work investigated a method of fabrication of NP of Co-ZnO and of Co with Si that would possibly have the desired properties by combining surface plasmon resonance due to high refractive index and magnetic material.

Fabrication of these NP involved two main steps: the deposition of a thin film via magnetron sputtering followed by the laser ablation of these thin films producing NP. The idea of this process was to have precise control of the chemical composition and to allow the formation of metastable phases. Structural (XRD, SAED), chemical (SIMS and EDS) and optical characterizations (Raman spectrometry) were conducted to verify the materials and properties at each step.

In conclusion, Co-ZnO were successfully synthesized with magnetron sputtering. This technique enabled the production of well-defined layers of ZnO and Co. On the other side, we did not manage to create a nanoparticle with a 3D web of Co inside of a ZnO matrix. A possible strategy to achieve this structure would be decreasing the thickness of the Co layer to have small agglomerations of Co. Laser ablation should be conducted in vacuum to avoid Co oxidation.

The Co-Si thin film deposition was not successful. Si content was far below the planned in the thin film. The NP, as expected with the thin film results, were all oxidized Co. A change to radiofrequency magnetron sputtering could allow a better sputtering of Si. As well as for the Co-ZnO system, the laser ablation should be conducted in vacuum.

REFERENCES

[1] Ecole Polytechnique Federale de Lausanne. A low-energy optical circuit for a new era of technology. **Phys Org**, Sep. 8, 2014. Available at <https://phys.org/news/2014-09-low-energy-optical-circuit-era-technology.html>. Access on: Nov. 23, 2020.

[2] Stanciu, C. D. *et al.*All-optical magnetic recording with circularly polarized light. *Phys. Rev. Lett.* **99**, 1–4 (2007).

[3] Rios, C. *et al.* Integrated all-photonic non-volatile multi-level memory. *Nat. Photonics* **9**, 725–732 (2015).

[4] Sasikala, V. & Chitra, K. All optical switching and associated technologies: a review. *J. Opt.***47**, 307–317 (2018).

[5] W.S. Fegadolli, L. Feng, M.M. Rahman, J.E.B. Oliveira, V.R. Almeida, A. Scherer, Experimental demonstration of a reconfigurable silicon thermo-optical device based on spectral tuning of ring resonators for optical signal processing, Opt. Exp. 22 (3) (2014) 3425.

[6] T. Miyazaki, R. Hasegawa, H. Yamaguchi, H. Oh-oka, H. Nagato, I. Amemiya, S. Uchikoga, Electrical control of plasmon resonance of gold nanoparticles using electrochemical oxidation, J. Phys. Chem. C 113 (19) (2009) 8484 .

[7] V.R. Almeida, C.A. Barrios, R.R. Panepucci, M. Lipson, All-optical control of light on a silicon chip, Nature 431 (7012) (2004) 1081 .

[8] V. Bonanni, S. Bonetti, T. Pakizeh, Z. Pirzadeh, J. Chen, J. Nogués, P. Vavassori, R. Hillenbrand, J. Åkerman, A. Dmitriev, Designer magnetoplasmonics with nickel nanoferromagnets, Nano Lett. 11 (12) (2011) 5333 .

[9] Mie, G. Beiträge zur Optik trüber Medien, speziell kolloidaler Metallösungen. *Ann. Phys.***330**, 377–445 (1908).

[10] Mie, G. & Newman, P. Contributions on the optics of turbid media, particularly colloidal metal solution - Translation. (1978)

[11] Kuznetsov, A. I., Miroshnichenko, A. E., Fu, Y. H., Zhang, J. et Luk'yanchuk, B. Magnetic light. *Sci. Rep.*, **vol. 2**, p. 492 (2012).

[12] Musorin, A. I., Barsukova, M. G., Shorokhov, A. S., Luk'yanchuk, B. S. & Fedyanin, A. A. Manipulating the light intensity by magnetophotonic metasurfaces. *J. Magn. Magn. Mater.***459**, 165–170 (2018).

[13] Golla, C., Weber, N. & Meier, C. Zinc oxide based dielectric nanoantennas for efficient nonlinear frequency conversion. *J. Appl. Phys.***125**, (2019).

[14] Sánchez Zeferino, R., Barboza Flores, M. & Pal, U. Photoluminescence and raman scattering in ag-doped zno nanoparticles. *J. Appl. Phys.***109**, (2011).

[15] Hasuike, N. *et al.* Structural properties of nanometre-sized ZnO crystals doped with Co. *J. Phys. Condens. Matter* **19**, (2007).

[16] Khorsand Zak, A., Razali, R., Abd Majid, W. H. & Darroudi, M. Synthesis and characterization of a narrow size distribution of zinc oxide nanoparticles. *Int. J. Nanomedicine* **6**, 1399–1403 (2011).

[17] Ansari, S. M. *et al.* Cobalt nanoparticles for biomedical applications: Facile synthesis, physicochemical characterization, cytotoxicity behavior and biocompatibility. *Appl. Surf. Sci.***414**, 171–187 (2017).

[18] Paul, A. The Kirkendall Effect in Solid State Diffusion PhD Thesis Laboratory of Materials and Interface Chemistry. (2004).

[19] Weaver, L., Simard-Normandin, M., Naem, A. & Clark, A. The Use of Tem and Raman Spectroscopy to Determine the Absorption Coefficient and Silicidation Sequence of Cobalt Silicide. *MRS Proc.***260**, 287–291 (1992).

[20] Liu, F. M. *et al.* Raman spectroscopic studies of the formation processes of cobalt suicide thin films. *Thin Solid Films***471**, 257–263 (2005).

[21] Larchev, V. I. & Popova, S. V. The new chimney-ladder phases Co2 Si3 and Re4 Ge7 formed by treatment at high temperatures and pressures. *J. Less-Common Met.***84**, 87–91 (1982).

[22] Balasubramanian, B. *et al.* Unusual spin correlations in a nanomagnet. *Appl. Phys. Lett.***106**, (2015).

[23] Serra, P. & Piqué, A. Laser-Induced Forward Transfer: Fundamentals and Applications. *Adv. Mater. Technol.* **4**, 1–33 (2019).

[24] Tajik, M. *et al.* Fabrication of spherical GeSbTe nanoparticles by laser printing technique. *J. Phys. Conf. Ser.* **917**, (2017).

[25] Zywietz, U., Evlyukhin, A. B., Reinhardt, C. & Chichkov, B. N. Laser printing of silicon nanoparticles with resonant optical electric and magnetic responses. *Nat. Commun.* **5**, 1–7 (2014).

[26] Larin, A. Private communication. Message received by <alexandre.nomine@univ-lorraine.fr> on Dec. 3, 2019.

[27] Diallo, A., Beye, A. C., Doyle, T. B., Park, E. & Maaza, M. Green synthesis of Co3O4 nanoparticles via Aspalathus linearis: Physical properties. *Green Chem. Lett. Rev.***8**, 30–36 (2015).

[28] Tang, C. W., Wang, C. Bin & Chien, S. H. Characterization of cobalt oxides studied by FT-IR, Raman, TPR and TG-MS. *Thermochim. Acta***473**, 68–73 (2008).

[29] Reinig, P., Fenske, F., Fuhs, W. & Selle, B. Crystalline silicon films grown by pulsed dc magnetron sputtering. *J. Non. Cryst. Solids***299**–**302**, 128–132 (2002).

[30] Márquez, E., Blanco, E., García-Vázquez, C., Díaz, J. M. & Saugar, E. Spectroscopic ellipsometry study of non-hydrogenated fully amorphous silicon films deposited by room-temperature radio-frequency magnetron sputtering on glass: Influence of the argon pressure. *J. Non. Cryst. Solids* **547**, 120305 (2020).